Supplemental Figure S1. Heat maps showing normalized expression of conserved and species-specific miRNAs in *Asparagus.*

miRNA abundances were assessed using the small RNA data from vegetative tissues, male flowers, female flowers, anthers, degenerate pistils from male flower, and fertile pistils from female flowers; all libraries were normalized to transcripts per 30 million reads (TP30M). Lineage- or species-specific miRNA candidates have the "cand" prefix in their names. Reproductive phasiRNA triggers miR2118 and miR2275 are highlighted by blue and orange sidebars. All miRNAs are hierarchically clustered based on abundances across tissues as indicated by the tree at the left (split across the two portions) using the "single" method and "Euclidean" distances.

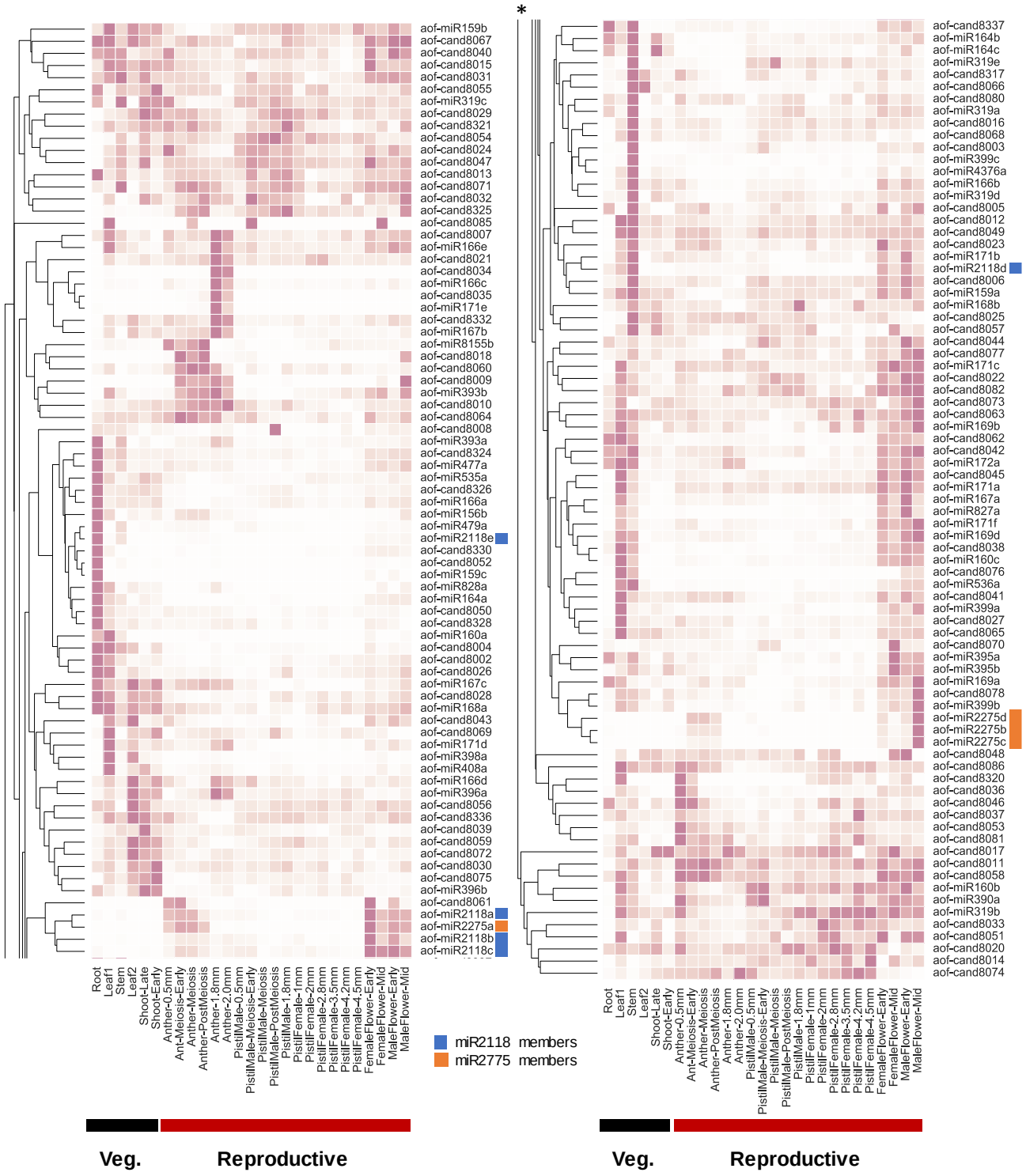

Supplemental Figure S2. miRNA abundances in *Asparagus* flowers, and phasiRNAs in female pistils.
(*A*) Heat map representing the Pearson's correlation values for an all-versus-all comparison of miRNA abundance levels in developmental stages of anther and degenerated pistils from male flowers. The pistil length corresponds to the stage of the anther of that specific length. (*B*) The miR2118 family in *Asparagus*, with heat-map showing enrichment or depletion in reproductive tissues relative to the leaf samples; variants of miR2118d are described in the main text. The numbers represent enrichment level in log(2) scale, as indicated above. The abundance counts for each mature variant and member are in Table S2. Solid lines in phylogenetic tree represents genomic variants of miR2118 family while the dotted lines represents transcriptional variants of miR2118d found in sRNA libraries. (*C*) Venn diagrams show counts of 24-nt *PHAS* loci identified in aborted male pistils and fertile female pistils, and their overlap with the set of 24-nt *PHAS* loci from anthers of male flowers. (*D*) Bar plots showing enrichment of 24-nt phasiRNAs, tasiRNAs, and hc-siRNAs in fertile pistils, represented in a log(2) scale.

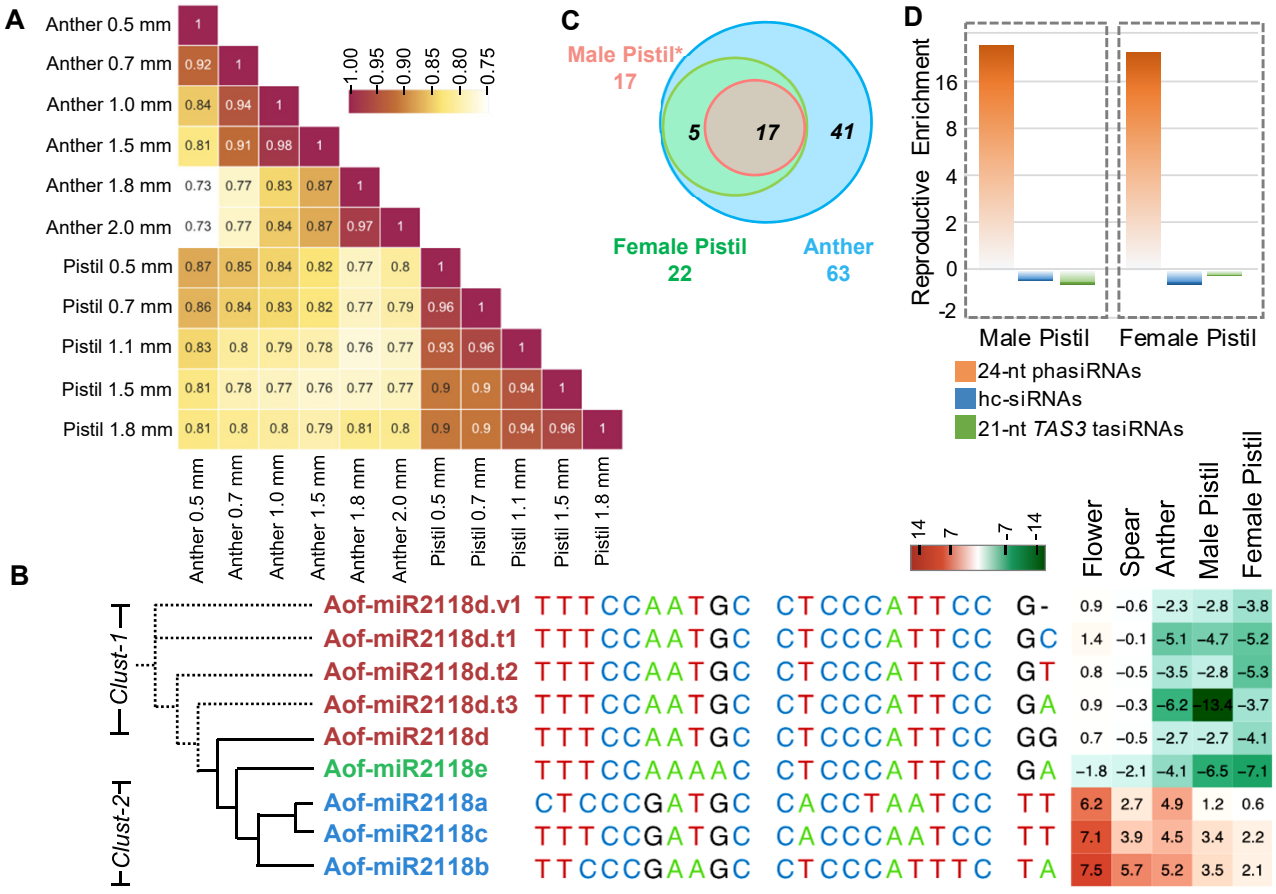

Supplemental Figure S3. Genomic organization and abundances of known and novel miRNAs in the *Asparagus* genome.

miRNAs were mapped to the *Asparagus* genome with chromosomes as indicated at right, and the abundance of each miRNA is displayed in a dot with the size indicated in a Log10 scale. The miR2118 family is encoded at three loci and the miR2275 family is encoded in a single cluster on chromosome 4. The Y-axis is a representation of coordinates listed in Supplemental Table S2.

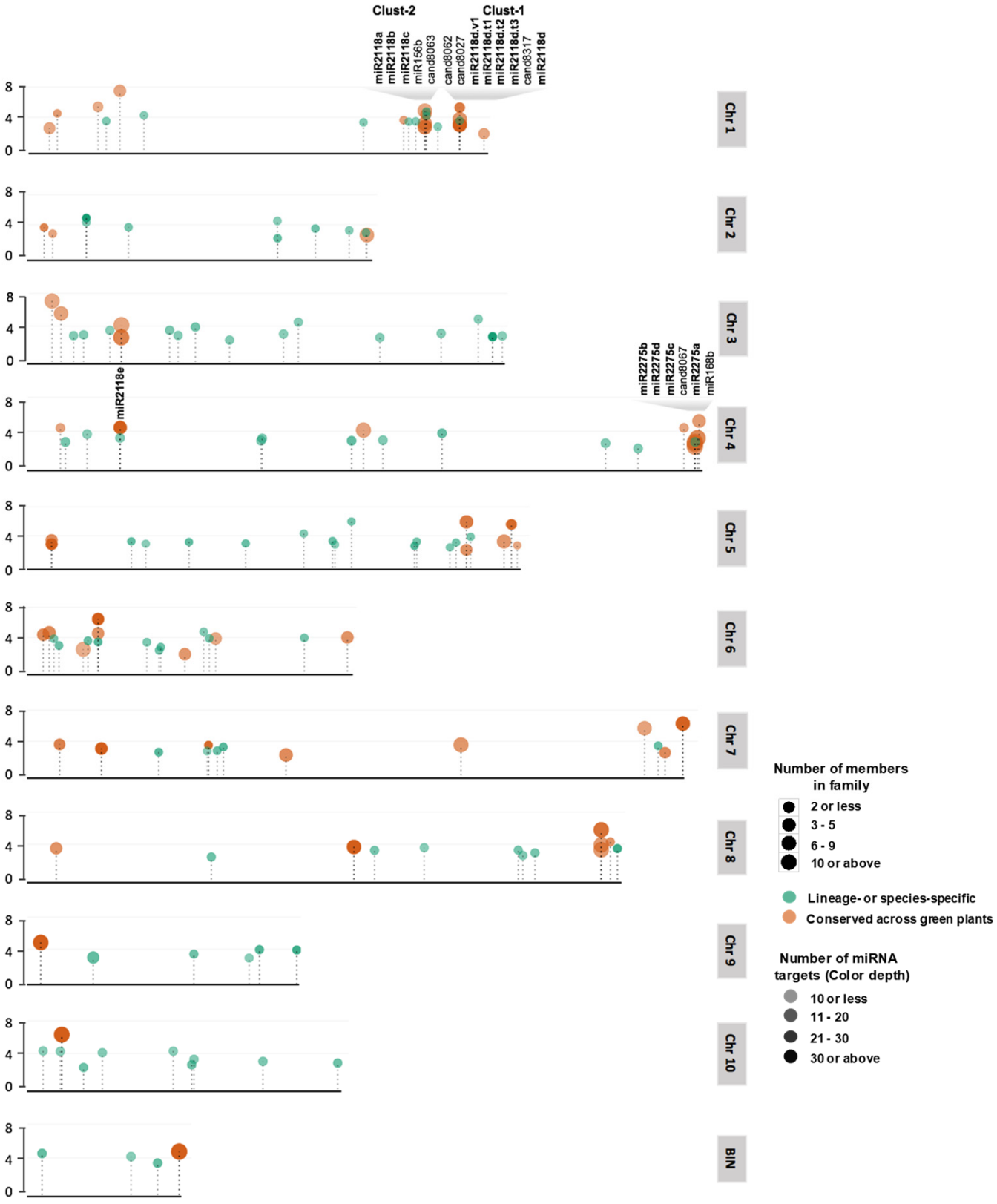

Supplemental Figure S4. Secondary structure and small RNA abundance plots of three representative foldback *PHAS* loci from *Asparagus*.

Foldbacks from unspliced genomic sequence display 24-nt siRNAs from both arms, at 24-nt intervals, a processive signature of Dicer activity. Inset scatterplots depict the sRNA distribution on *PHAS* transcripts, starting from the 5'-most 24-nt phasiRNA. The abundance is indicated on the Y-axis, shown in log2 scale, and axis limits set to 40, 10 and 20 for 24-*PHAS*-23, 24-*PHAS*-3 and 24-*PHAS*-26 respectively. The position of the first and last phasiRNAs for the 5'- and 3' arms, along with the total phases and arm lengths, are described in the header of each scatterplot. The dot colors and sizes represent sRNA sizes and abundances, respectively.

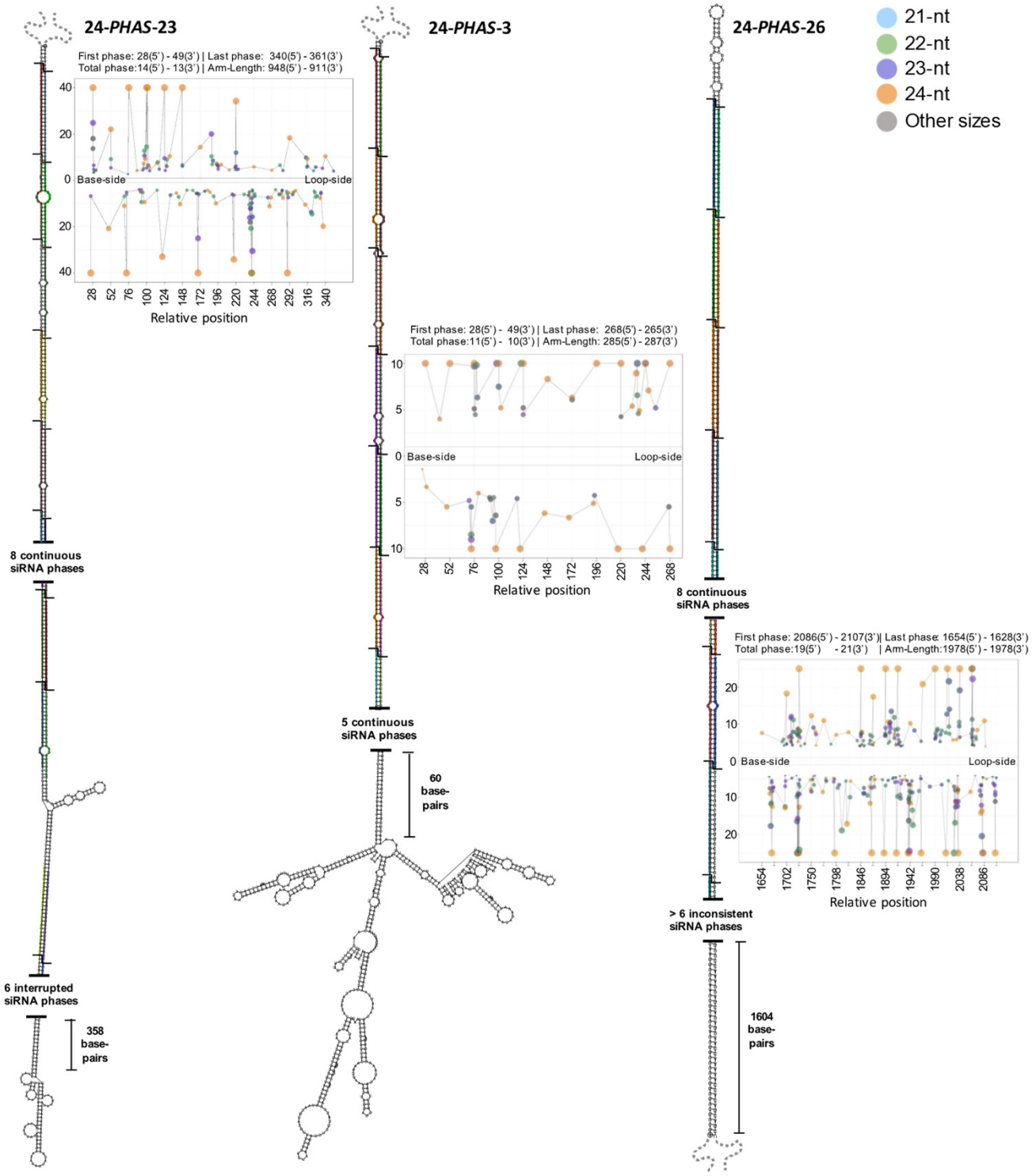

Supplemental Figure S5. 24-nt *PHAS* loci in maize, derived from inverted repeats.
(A) Maize cluster-125, with two 24-nt *PHAS* loci precisely located at edges of the 5' and 3' arms of a 9433-nt inverted repeat, and flanked by 24-nt loci that are direct repeats. Inset images are screenshots of our browser showing the phasing scores of 24-nt sRNAs from this region with the red dot indicating the maximum score and orange dots are sRNAs in phase (grey are out of phase). Red or blue boxes are annotated genes on the top or bottom strand; orange cross-hatched boxes indicate that we have marked this as a 24-nt *PHAS* locus. Positions are from version 2 of the maize genome. *(B)* Maize cluster-19 is a *PHAS* locus with an internal foldback structure, but flanked by another 24-nt *PHAS* locus on left, both are located in the 5' and 3' arms of a fragmented but longer inverted repeat. The distance between *PHAS* loci in *(A)* and sequence similarity between the 5' and 3' arms of a longer inverted-repeat in *(B)* suggest that these longer inverted repeats are likely disrupted during evolution. Small RNA libraries for maize meiotic anthers from Zhai *et al.* (2016) were used for these plots.

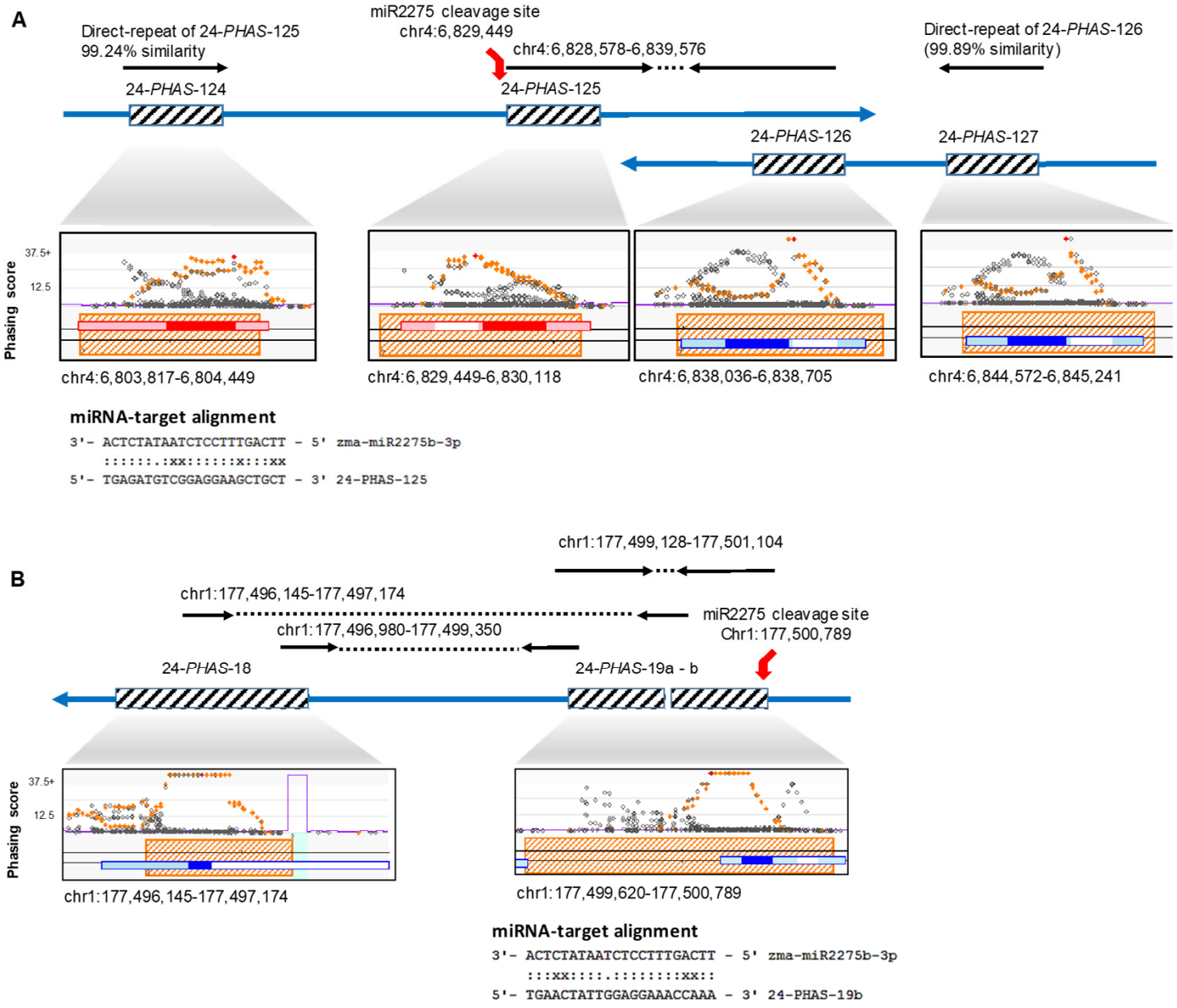

Supplemental Figure S6. Secondary structure of a foldback transcript from a 21-*PHAS* locus from *Asparagus*.

Secondary structure of the *Asparagus* 21-*PHAS*-10 precursor identified from the transcriptome assembly. Phased siRNAs initiate from the miR2118 cleavage site; these are denoted with varying colors (visible at a high level of magnification, but indicated with hash marks). Two transcript variants were identified, both likely processed from base-to-loop direction, generating phasiRNAs corresponding to both arms, from 15 contiguous cuts, followed by at least 8 more cuts. The precursors transcripts spanned a ~88 kb genomic region, overlapping at least three transcribed loci (non-coding and of unknown coding potential), not shown here but located in the *Asparagus* genome (version 1.1) on chromosome 3 from 103,555,887 to 103,643,976.

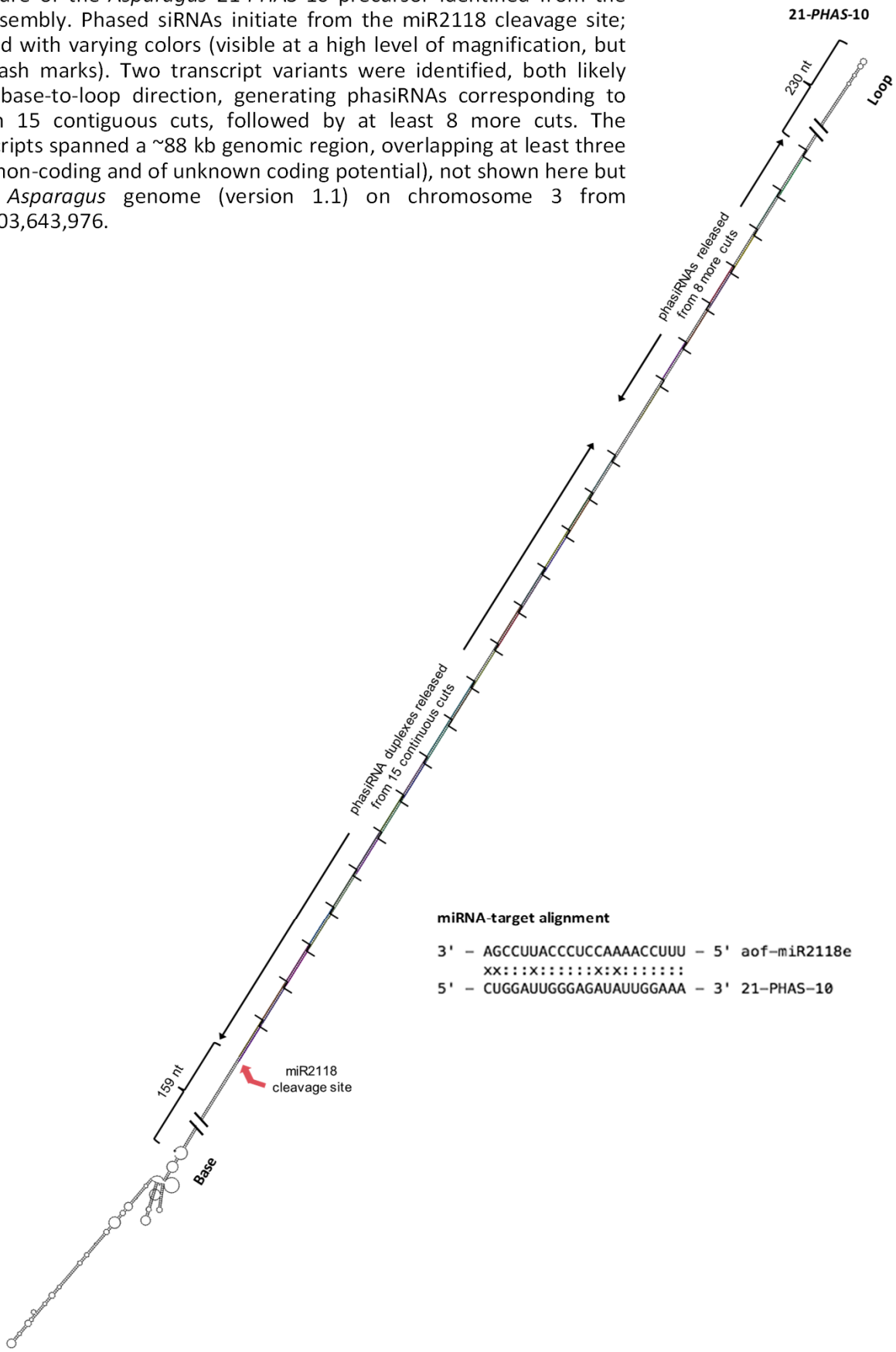

Supplemental Figure S7. Anther stage and size correlations capture pre-meiotic and meiotic anther stages for *Lilium* and daylily.

(A) Paraffin-embedded *Lilium* samples, cross-sectioned and stained with propidium iodide. Histology and cell divisions were examined for determination of the cell stages using confocal microscopy. Based on the morphology of archesporial cells (yellow arrows), 4 mm and 5 mm anthers corresponded to pre-meiotic stages. The 6 mm and 7 mm anthers were undergoing meiosis, and displayed a well-developed tapetum. *(B)* For daylily, anthers were treated with ScaleP clearing buffer for 1 week (see methods), and imaged using confocal microscopy. Histology and cell divisions in the longitudinal images of anthers were examined for determination of stages; the 1 mm anther was at a pre-meiotic stage, while 2 mm and 3 mm anthers were past meiosis and the tapetum was starting to thin out. Scale bars = 100 µm for all images.

A

Size	**4 mm**	**5 mm**	**6 mm**	**7 mm**
Stage	Pre-meiosis	Pre-meiosis	Meiosis I	Meiosis II
Number of cell layers	NA	5	5	5
Tapetum	NA	Formed, intact	Intact	Start to thin out

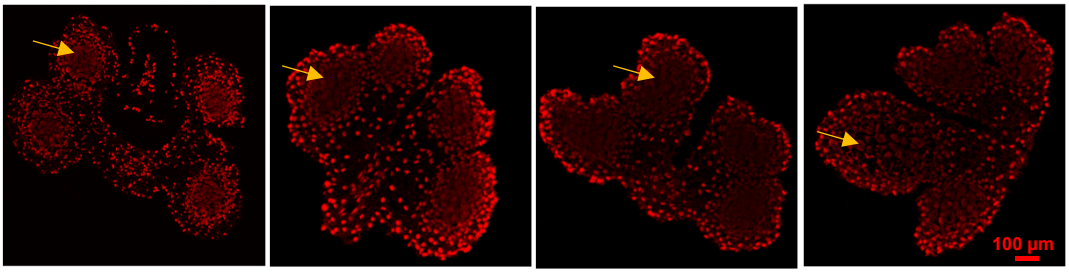

B

Size	**1 mm**	**2 mm**	**3 mm**
Stage	Pre-meiosis	Post-meiosis (indicated by filled anthers)	Pollen developed
Number of cell layers	5	4	4
Tapetum	Formed	Thinning	Thinned out

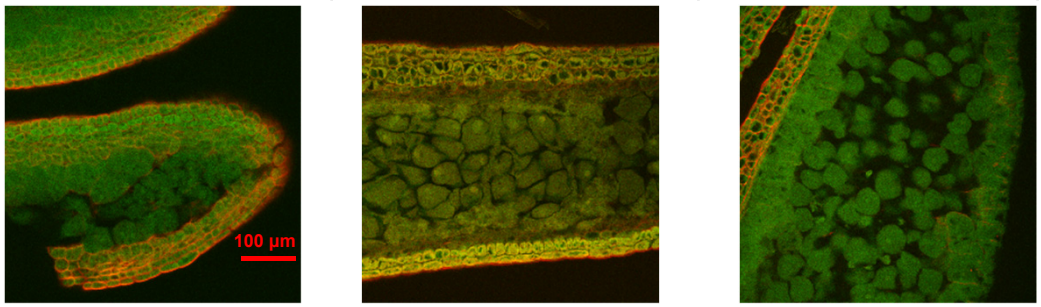

Supplemental Figure S8. Transcriptome and hybrid assemblies developed for *Asparagus, Lilium* and daylily. Precisely-staged pre-meiotic, meiotic anther and leaf samples were used to generate transcriptome assemblies for *Lilium* and hybrid assemblies for *Asparagus* and daylily; a phylogeny of species is at left and data types and metrics at right. For single- and paired-end libraries, reads are represented in million(s), and for SMRT libraries processed full-length transcripts are represented in thousands. The E90N50 metric signifies the N50 statistic for transcripts in the 90th percentile of normalized expression.

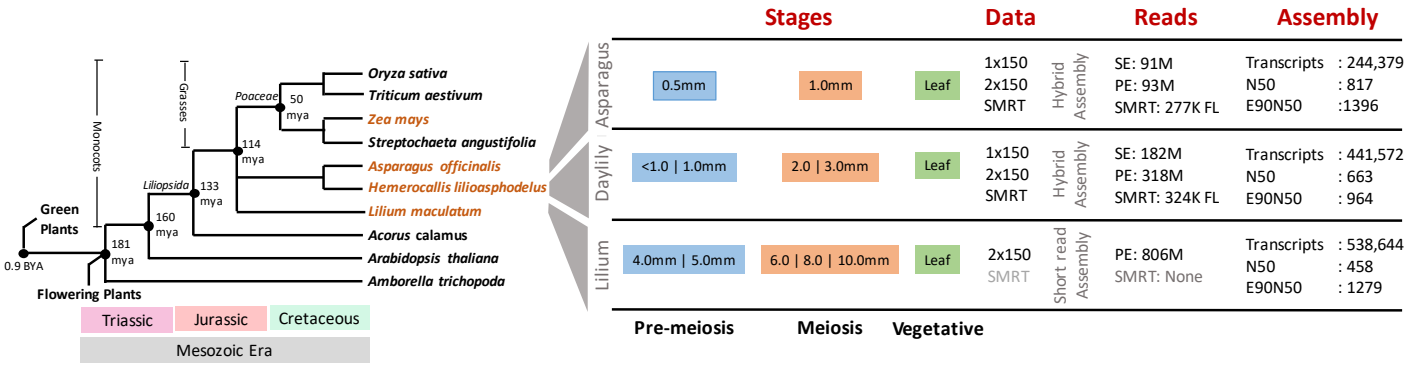

Supplemental Figure S9. Daylily 24-nt phasiRNAs and miR2275 are abundant in meiotic-stage anthers.
Heat maps depicting abundance of daylily 24-nt phasiRNAs (in red) and the miR2275 trigger family (in blue) in developing anther. Both heat maps are clustered on similarity of expression. Pie charts represent the proportion of stage-specific abundances for 24-nt phasiRNAs (in red), miR2275 (in orange) and and miR390 (the trigger of *TAS3* tasiRNAs, in green) across different anther developmental stages that are included in this study. The box-whisker plot shows the enrichment (log2) of daylily 24-nt phasiRNA abundance from all *PHAS* loci in the meiotic anther compared to the vegetative sample (leaf).

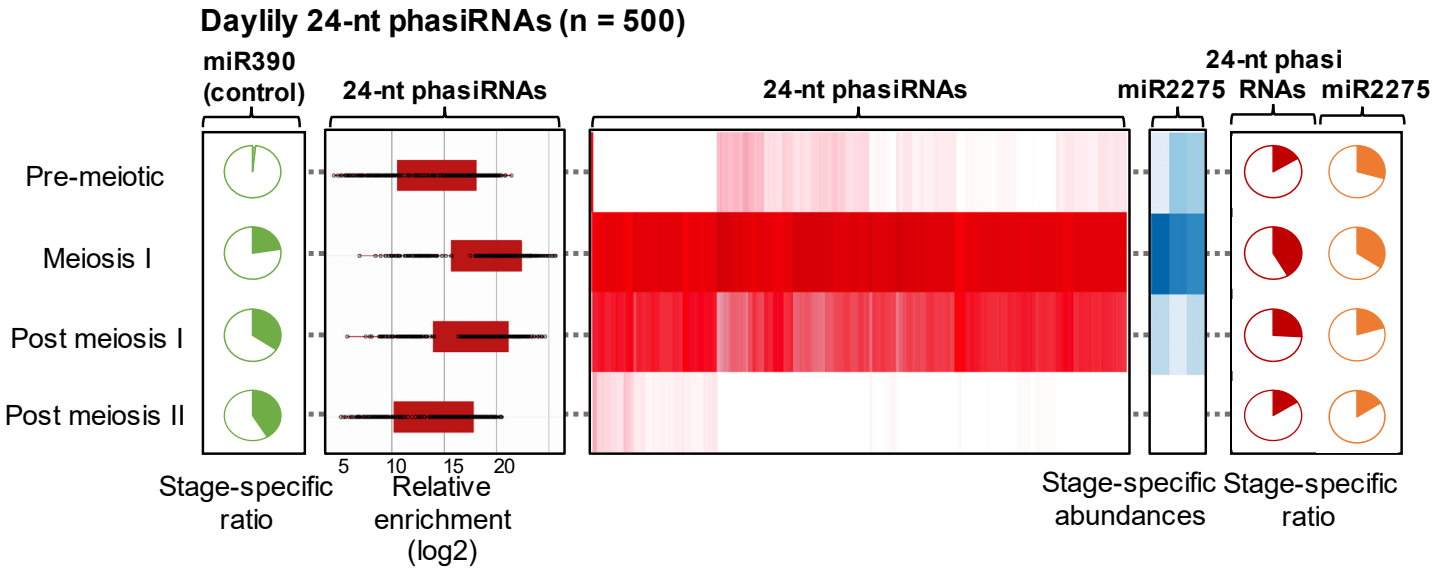

Supplemental Figure S10. Secondary structure and sRNAs for three representative foldback *PHAS* precursors from *Lilium*.

Precursors display consistent production of 24-nt long siRNAs from both arms, at 24-nt intervals, a processive signature of DCL5 activity. Scatter-plot depicts sRNA distribution on *PHAS* precursor transcripts, starting from the first detected 24-nt phasiRNAs. The abundance, on Y-axis, is shown in log2 scale. Position of first and last phasiRNAs for 5'- and 3'-arm along with the total phases and arm lengths are described in header of each scatter plot. The colors and size, in scatter plot, represent sRNA size class and abundance respectively.

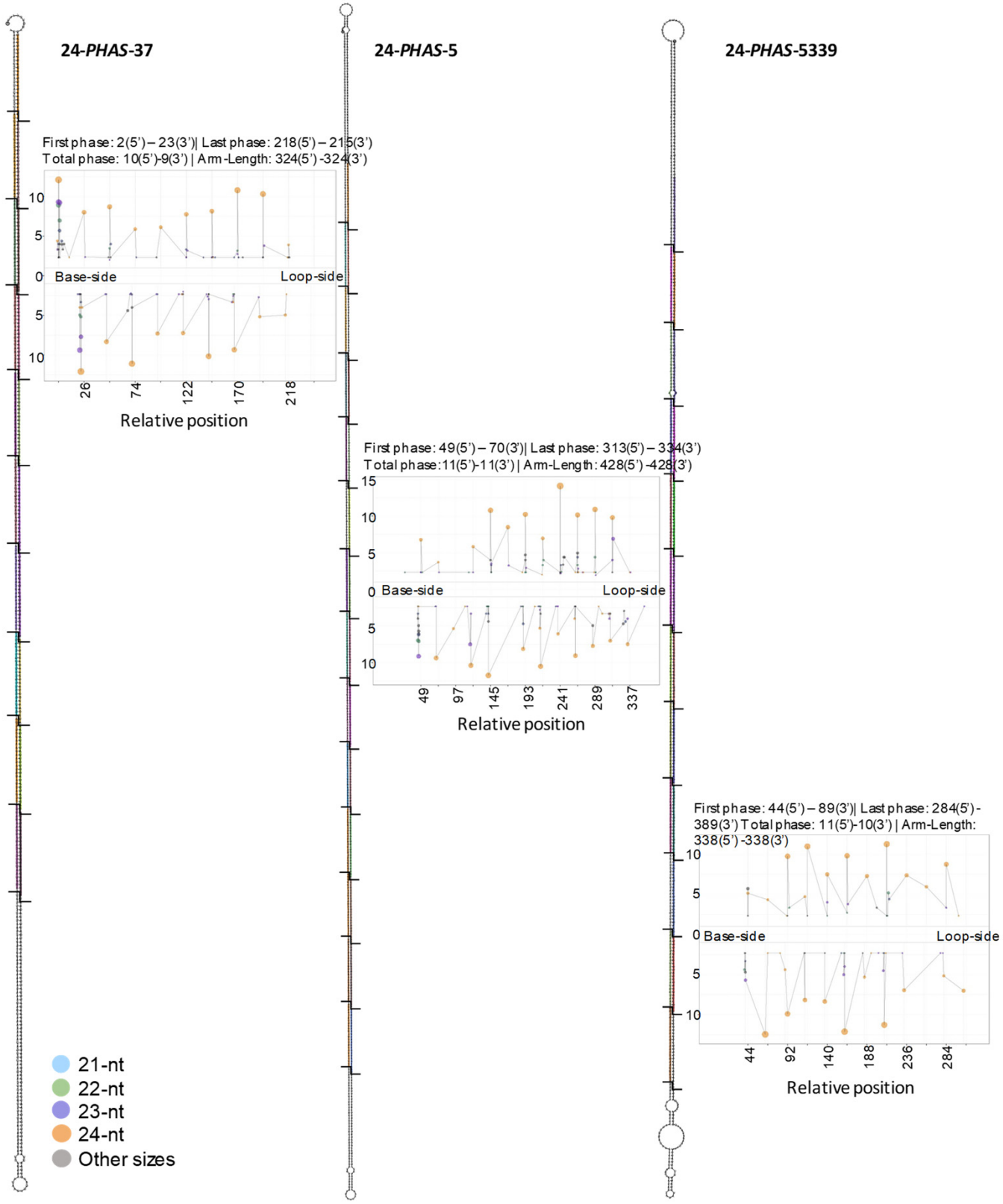

Supplemental Figure S11. Localization of 24-nt phasiRNA components in premeiotic (~4 mm) and meiotic (~5 mm) anthers of *Lilium*.

Small RNA *in situ* hybridizations in pre-meiotic and meiotic anthers of *Lilium*, using probes for miR2275 and, meiotic phasiRNAs and precursor transcripts from foldback 24-*PHAS*-5505 and IR-type 24-*PHAS*-5843. Meiotic anthers were used for these *in situ* hybridizations. 24-nt phased siRNAs were not detected at the pre-meiotic stage.

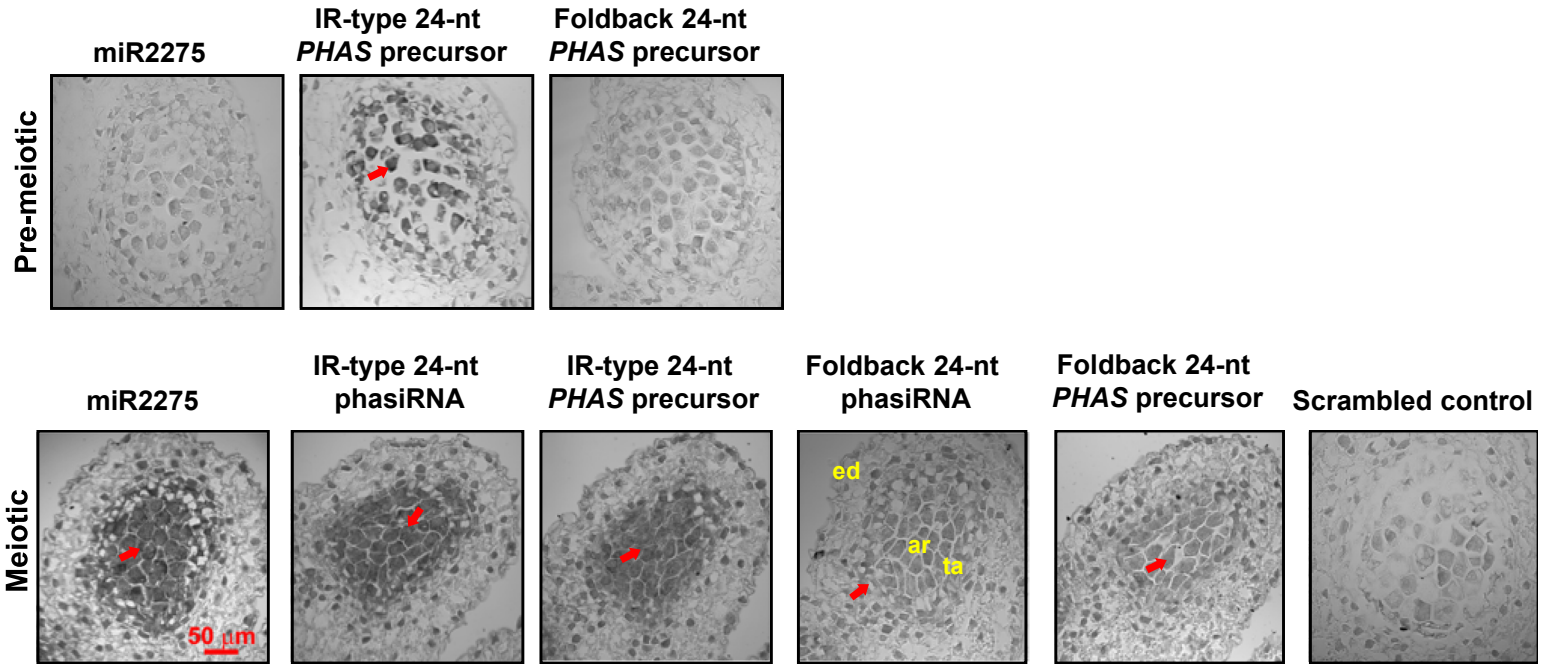

Supplemental Figure S12. First cycle, lower strand small RNAs from foldback *24-PHAS* transcripts are highly variable in length.

The proportion of 24-nt phasiRNAs abundances (orange) compared to other small RNA size classes (blue) in miR2275-triggered foldback *PHAS* precursor transcripts. P1 to P8 represents first eight phasiRNA sites or cycles in the precursor. Foldback precursors with a miR2275 target site are predicted to initiate precisely at P1 as a result of miRNA-directed cleavage; this analysis was conducted using a representative set of loci (n=18). Data for this figure is provided in Supplemental Table S15.

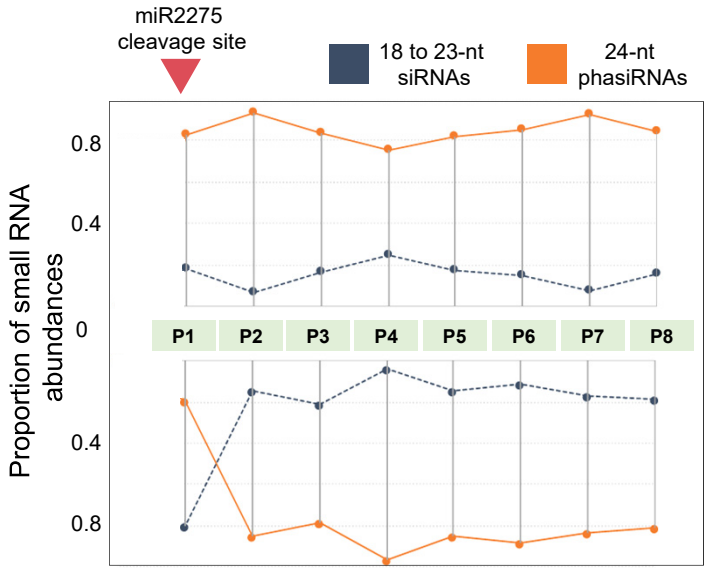

Supplemental Figure S13. Levels of IR-derived small RNAs are reduced in a *dcl1* mutant in Arabidopsis. *(A)* Pie charts represent small RNA abundances of 21- to 24-nt sizes derived from *IR-71* and *IR-2039,* endogenous IR loci in Arabidopsis. Counts represents the normalized abundance in thousands. *(B)* Heat maps representing differential abundance of 21-, 22-, 23- and 24-nt sRNAs in Arabidopsis mutants *dcl3-1, dcl2-1/dcl3-1/dcl4-2*, *dcl1-7*, *nrpd1a-4*, *rdr2* and *nrpe1-11* relative to wild-type levels. Allele numbers were left out of the figure to save space.

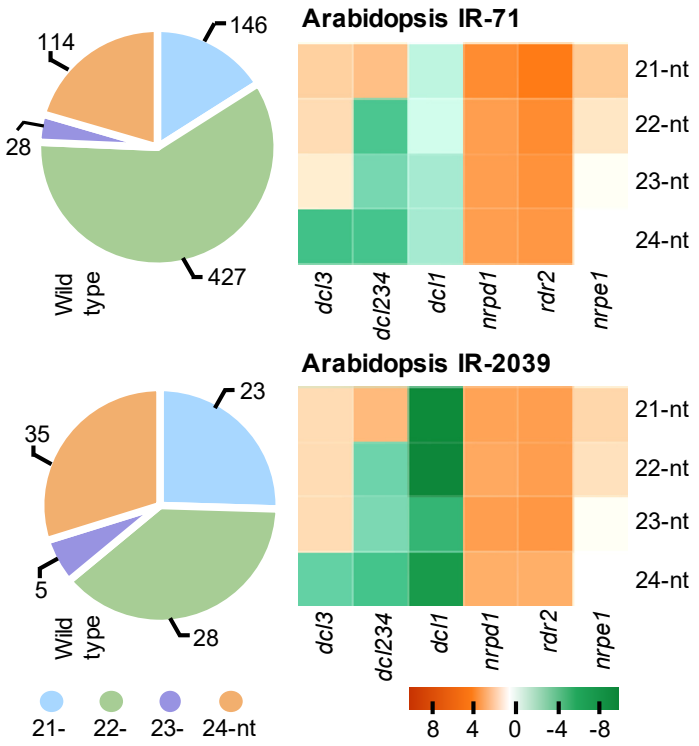

Supplemental Figure S14. *Dicer-like* (*DCL*) and Argonaute gene family members in *Asparagus*, daylily and *Lilium*. *(A)* Phylogenetic tree of *AGO* members from *Asparagus* (Ao), daylily (Hl) and *Lilium* (La) identified in this study along with four representative species: Arabidopsis (At), rice (Os), maize (Zm) and soybean (Gm). The *AGO9* family was renamed to *AGO4* because these are closely related in many plants. *(B)* A Dicer phylogeny with members from *Asparagus* (Ao), daylily (Hl) and *Lilium* (La) identified in this study along with four representative species – Arabidopsis (At), rice (Os), maize (Zm) and soybean (Gm). *(C)* Bar plots representing the relative expression of *DCL5* in *Asparagus* pre-meiotic & meiotic anthers, and leaves, as measured by quantitative, real-time PCR. Measurements were from six biological replicates; bars indicate the standard error.